Nonequilibrium Dynamics in Amorphous $Si_3B_3N_7$

A. Hannemann, J. C. Schön,* and M. Jansen

Max Planck Institut für Festkörperforschung, Heisenbergstrasse 1, D-70569 Stuttgart, Germany

P. Sibani

Fysisk Institut−SDU, Campusvej 55, DK-5230 Odense, Denmark

Received: February 2, 2005; In Final Form: April 14, 2005

We present extensive numerical investigations of the structural relaxation dynamics of a realistic model of the amorphous high-temperature ceramic a-$Si_3B_3N_7$, probing the mean-square displacement of the atoms, the bond survival probability, the average energy, the specific heat, and the two-point energy average. Combining the information from these different sources, we identify a transition temperature $T_c \approx 2000$ K below which the system is no longer ergodic and physical quantities observed over a time t_{obs} show a systematic parametric dependence on the waiting time t_w, or age, elapsed after the quench. The aging dynamics "stiffens" as the system becomes older, which is similar to the behavior of highly idealized models such as Ising spin glasses and Lennard-Jones glasses.

Introduction

The physical aging of polymers and other "soft" materials was studied experimentally almost three decades ago by Struik and co-workers.[1,2] The interest of a wider community for this area was then greatly stimulated by the work of Lundgren et al.[3] on the magnetic properties of spin glasses, and aging has since remained a source of important questions and insights in nonequilibrium statistical physics.[4]

The basic features of aging were mainly established during the 1980s in studies of the magnetic linear susceptibility and autocorrelation functions of spin glasses[5−8] but are shared by many other systems, including, to cite only a few examples, type II superconductors,[9] glasses,[10−14] granular materials,[15] and soft condensed matter.[16] After a rapid quench of a relevant parameter, e.g., when the temperature of a glass is rapidly lowered below a threshold value, aging materials are unable to reequilibrate within the available observation time. What is observed is a slow change of physical properties that occurs at a decelerating pace and in a fashion largely independent of most details of the microscopic interactions. More precisely, physical observables systematically depend on the system age t_w, i.e., the time elapsed from the initial quench, and the observation time t_{obs}. On the basis of the relative values of t_w and t_{obs}, two dynamic regimes can be identified: For $t_{obs} \ll t_w$, macroscopic physical averages are approximately constant, and two-time correlations are related to the linear response through the fluctuation−dissipation theorem. Such a "quasi-equilibrium" regime strongly resembles the time translational invariant dynamics of thermal equilibrium, except for the fact that many quantities, e.g., relaxation times, can carry a parametric age dependence. For $t_{obs} \gg t_w$, physical averages visibly drift and two-time averages no longer obey the fluctuation−dissipation theorem.

Recent improvements in time-resolved spectroscopic techniques[17−20] have highlighted that, far from being a smooth flow, the drift of aging systems results from a highly irregular, so-called *intermittent*, process, whereby sudden and large configurational rearrangements[21] punctuate the prevailing equilibrium-like fluctuations. These intermittent events may correspond to irreversible jumps from one metastable state to the next.[22,23]

Aging has raised a wealth of theoretical questions, for example, whether the nonequilibrium aging regime can be described through the concept of effective temperature.[24,25] Of direct relevance for the present investigations is the origin of the so-called pure aging behavior, i.e., the t_{obs}/t_w scaling of various observables in the aging regime[21,26] and of modified scalings,[27] which are called subaging and super- or even hyperaging.

This work discusses numerical investigations of the dynamic and thermodynamic properties of a *realistic* model of a-$Si_3B_3N_7$ for a large temperature range. The material is representative of a class of nitridic ceramics with chemical composition a-$Si_xB_yN_1C_z$,[28−37] which can be synthesized via the sol−gel process.[33] These ceramics are of great technological interest and are presently considered for high-temperature engine applications.

Nitridic ceramics appear to form amorphous covalent networks with a homogeneous distribution of the cations at least down to a scale of 1 nm.[38] Experimental studies have mainly focused on the quaternary compound a-$SiBN_3C$. Under standard conditions, both a-$SiBN_3C$ and a-$Si_3B_3N_7$ are thermally stable and amorphous up to very high temperatures, e.g., about 2100 K for a-$SiBN_3C$. They possess excellent mechanical and elastic properties, e.g., a-$SiBN_3C$ has a high bulk modulus of ca. 200−300 GPa and is stable against oxidation up to 1700 K.

The amorphous structure suggests a similarity with glassy materials and hence the presence of aging properties of potential technological relevance. Probing the glass transition of, e.g., a-$Si_3B_3N_7$, the basic representative of this class of nitridic ceramics, is impossible at standard conditions, since decomposition takes place at $T \approx 1900$ K, i.e., well before the ceramic melts. However, the melting transition might be accessible, as we have argued, at very high pressures.[39]

* Author to whom correspondence should be addressed. E-mail: schoen@fkf.mpg.de.

10.1021/jp050586h CCC: $30.25
Published on Web 05/19/2005

The Monte Carlo (MC) simulations presented below aim for the determination of the temperature range below which the nonergodic behavior of a-$Si_3B_3N_7$ sets in and the characterization of the aging dynamics in that low-temperature regime. Admittedly, determining "for all practical purposes" whether a system is ergodic or not is not straightforward and is possibly an ill-posed question.[40] As will become clear from the discussion, we refer to nonergodic behavior as a collection of dynamic properties usually associated with glassiness, which, taken together, describe a strong deviation from thermal equilibrium.

To detect the onset of ergodicity breaking and characterize the behavior in both the ergodic and nonergodic regions, we consider a number of relevant dynamic and thermodynamic measures: (1) The physical movement of the particles, as statistically characterized by the mean-square displacement (MSD), is diffusive in the ergodic region and subdiffusive elsewhere. (2) The related bond survival probability (BSP)[41] drops to a finite average close to zero on a characteristic time scale at sufficiently high temperatures but becomes scale-free and age-dependent in the nonergodic region. There, it decreases as a logarithmic function of t_{obs}/t_w^{α}, where α is close to 1 and depends on the type of particles forming the bond. (3) The specific heat C_V is calculated in three different ways, which agree in equilibrium but markedly differ in the nonergodic region. (4) The two-time energy−energy average $\phi(t_w,t_{obs};T)$ defined in eq 6. By construction, ϕ equals 1 in equilibrium or in a quasi-equilibrium regime and is larger than 1 when the system is out of equilibrium. (5) The age dependence of the energies of the local minima or so-called inherent structures (IS)[42] characterizing the trajectories in the nonergodic regime. These energies decrease logarithmically with the age.

The rest of the paper is structured as follows: In section 2, we introduce the model and simulation technique. In section 3, we define the statistical measures used to probe the ergodicity breaking and present the corresponding results. Finally, section 4 contains a broader discussion of the results, where we show that our findings are in general agreement with previous studies of the aging dynamics of much simpler atomistic models[12,43,44] and also with experimental results in, e.g., spin glasses,[45] polymer systems,[2] and charge-density waves.[46]

2. Model and Techniques

The model of a-$Si_3B_3N_7$ consisted of 162 Si atoms, 162 B atoms, and 378 N atoms, respectively, in a 19.1 × 19.1 × 19.1 Å^3 cubic box. As an interaction potential, we employed a two-body potential from the literature[47] based on fits to ab initio energy calculations of crystalline and molecular compounds containing Si, B, and N atoms. This potential successfully reproduces experimental data regarding structural properties such as bond lengths and bulk properties, e.g., vibrational frequencies, of the binary compounds Si_3N_4 and BN and of molecules containing Si−N−B units.

The starting configurations for our simulations were generated by relaxation from high-temperature melts. The simulations were performed at fixed temperature and volume, with a Monte Carlo algorithm using the Metropolis acceptance criterion. In each update, an atom is randomly selected for an attempted move with a random direction and with an average size chosen to achieve an acceptance rate of ∼50%. One Monte Carlo cycle (MCC) corresponds to $N_{atom} = 702$ such individual moves. Note that the kinetic energy ($^3/_2 k_B T$ per atom) does not appear in MC simulations and that all quantities studied relate to the configurational energy. For comparison, we also performed molecular dynamics (MD) simulations in the melt. Comparing mean-square displacements determined from MD and MC simulations, respectively, we estimate that (at least in the high-temperature regime) one MCC corresponds to about 0.5 fs. At low temperature, the value of the microscopic time scale is not known precisely. However, this value is not crucial for the study of aging quantities, which, as in our case, have a logarithmic time dependence or depend on the ratio of two times.[48]

The temperatures investigated ranged from 25 to 10 000 K; however, for $T \leq 250$ K, no discernible dynamic evolution took place on the time scale of the simulations. For each temperature up to 3000 K and above 3000 K, 9 and 3 runs, respectively, of length $t_{total} = 2 \times 10^5$ MCC were performed.

The energy $E(t;T)$ as function of time was registered every 10 MCC. Along the individual trajectories for $T = 250$, ..., 7000 K, halting points x_H were chosen, from which conjugate gradient minimizations were performed. In the following, $t_{init} \approx 1000$ MCC is the initialization time of the MC simulations needed for the system to reach equilibrium in the ergodic regime (i.e., at high temperatures), while $t_w \geq t_{init}$ is the waiting time before the observations begin. Furthermore, an ensemble of 100 runs of length $t_{total} = 10^6$ MCC was studied, to investigate aging in greater detail and with better statistics. Each starting configuration of the ensemble was generated by quenching the system from 4000 to 1250 K. (Due to the rather expensive energy evaluation, performing the runs in this ensemble required approximately a computing time of 1 year on a AMD/1800 PC.)

The diffusivity of the atoms in the high-temperature regime was calculated straightforwardly from the mean-square displacement as a function of time via the Einstein−Smochulowski relation ($D \propto \mathrm{MSD}(t_{obs})/t_{obs}$). Finally, in the bond survival probability data, a B−N or Si−N bond was considered broken if the interatomic distance was above 2.0 Å.

In computing time averages and correlations, we considered the observation interval $I = [t_w, t_w + t_{obs}]$. Time averages over I are denoted by an overbar, while an angular bracket stands for an average over an ensemble of independent trajectories.

3. Ergodicity Breaking and Aging Behavior

3.1. Ergodicity Breaking. Evidence for ergodicity breaking can be extracted from a change of behavior in dynamic quantities, i.e., the MSD and BSP as well as from thermodynamical quantities, i.e., the heat capacity, the energy average, and the two-point energy average. All these data concur that ergodicity breaking occurs but differ to some degree with respect to the precise value of the transition temperature T_c. The latter can be approximately located within the range 2000−2500 K.

We consider the high-temperature behavior first. For $T > T' = 2100$ K, the MSD between pairs of time-displaced atom positions only depends on the length of the observation interval

$$\mathrm{MSD}(t_{obs},t_w) = \sum_i [\vec{r}_i(t_w + t_{obs}) - \vec{r}_i(t_w)]^2 \qquad (1)$$

$t_{obs} = (t_{obs} + t_w) - t_w$. The diffusion coefficients for the different atoms all have an Arrhenius temperature dependence, with activation barriers $\Delta E = 1.24 \pm 0.09$ eV and 1.27 ± 0.06 eV for silicon and boron atoms, respectively.

In the same regime, the BSP is age independent and has a finite relaxation time τ_{BSP}. The values of τ_{BSP} were obtained by fitting the time dependence of the bond survival probabil-

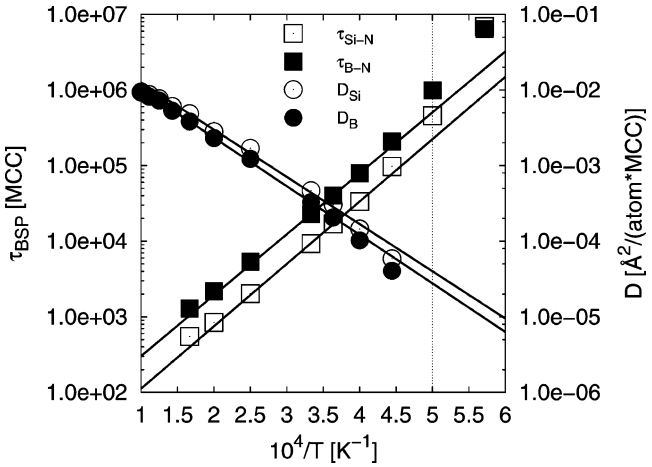

Figure 1. Temperature dependence of relaxation times τ_{BSP} for Si−N (empty squares) and B−N (filled squares) and temperature dependence of diffusion coefficients D(Si) (empty circles) and D(B) (filled circles). Straight lines show fits to an Arrhenius law. The dotted vertical line indicates the critical temperature $T_C \approx 2000$ K.

ity after the initialization time t_{init} to the Kohlrausch−Williams−Watts law[49]

$$\mathrm{BSP}(t,t_{\mathrm{init}};T) \propto \exp\left(-\left[\frac{t}{\tau_{\mathrm{BSP}}(T)}\right]^{\beta}\right) \qquad (2)$$

yielding exponents $\beta \approx 0.3-0.5$. The time scale $\tau_{BSP}(T)$ has an Arrhenius-like temperature dependence, with activation barriers $\Delta E = 1.64 \pm 0.02$ eV and 1.60 ± 0.02 eV for Si−N and B−N bonds, respectively. Arrhenius plots for the diffusion coefficients of silicon and boron atoms and for the relaxation times τ_{BSP} are plotted in Figure 1. A deviation from the Arrhenius scaling is apparent in both quantities as T approaches 2000 K from above.

The activation barriers found for both diffusion and bond breaking are in a similar range, suggesting that a single Arrhenius time scale might characterize the high-temperature dynamics. However, although diffusive processes need to be accompanied by bond breaking, it is not clear whether this effect or steric blocking by neighbor atoms dominates the diffusion at various temperature scales.

Deviations from activated behavior appear in the relaxation time as the temperature decreases. Approaching $T' \approx 2100$ K from above, the diffusion coefficients for B, Si, and N atoms all vanish for $T \to T'$ as $D \propto (T - T')^{\gamma}$ with $\gamma = 1.6$. A similar deviation of τ_{BSP} from an Arrhenius law is observed when $T'' \approx 1720$ K for B−N and $T'' \approx 1820$ K for Si−N, respectively, are approached from above. Close to these temperatures, $\tau_{BSP}(T)$ grows roughly like a power law: $\tau_{BSP}(T) \propto (T/T'' - 1)^{\delta}$ with $\delta_{B-N} \approx -2.5$ and $\delta_{Si-N} \approx -2.3$. At even lower temperatures, the particle motion becomes subdiffusive and the BSPs fall off logarithmically. Both quantities become scale-free but gain a characteristic age dependence, discussed in more detail in section 3.2.

Thermodynamical variables such as the specific heat C_V, the energy average, and a suitably normalized two-time energy−energy average ϕ require averaging over an ensemble. For a fixed amount of numerical effort, they are hence less precisely determined than "local" dynamic properties but offer nevertheless concurring insights into ergodicity breaking and aging behavior.

The heat capacity was evaluated with three different prescriptions, all agreeing in thermal equilibrium. Note that all specific

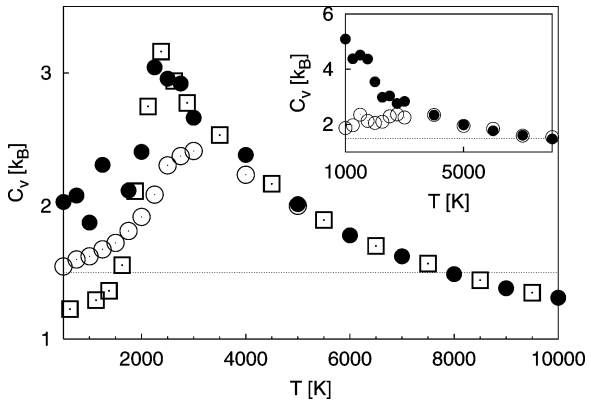

Figure 2. Temperature dependence of the specific heats per atom C_V^a (□), C_V^b (○), and C_V^c (●), for $T \in [500,10000]$ K. For C_V^a and C_V^c, the waiting time t_w and the observation time t_{obs} are both equal to 10^5 MCC. C_V^b is obtained by averaging over 10 equidistant t_w values over the interval 10^5 to 2×10^5, for each of three independent trajectories. The observation time was kept at $t_{obs} = 5 \times 10^3 \ll t_w$. All procedures agree for $T > 3000$ K, the region in which the system equilibrates according to this measure. Inset: For temperatures $T \in [1000,8000]$ K and waiting time $t_w = 10^4$, C_V^c is shown with symbols ○ and ● corresponding to observation times $t_{obs} = 10^4$ and $t_{obs} = 10^5$, respectively. The high values (●) at low temperatures seen for $t_{obs} \gg t_w$ are a consequence of the energy drift present in this dynamic regime. For the shorter observation time (○), the values are in good agreement with the C_V^b values shown in the main panel with the same symbol (note the difference in scale). The agreement expresses the equivalence between drift and fluctuation within the quasi-equilibrium low-temperature regime of the aging system.

heat data are reported on a per atom basis. The disagreement observed at lower temperature shows that the system is nonergodic for the observational time scale used. We note that agreement at higher temperatures does not neccessarily imply that the equilibrium state is reached,[50] since such an agreement is only a necessary but not a sufficient criterion for the system to be in equilibrium.

Our first prescription is naively carried over from equilibrium thermodynamics. Leaving the T dependence of the mean energy understood on the right-hand side of the equation, we define

$$C_V^{\,a}(T) = \frac{\partial \langle \overline{E} \rangle}{\partial T} \qquad (3)$$

where the temperature derivative is performed numerically after the ensemble and time averaging denoted by the broken brackets and an overbar, respectively.

Second, we consider simulations where the temperature is increased or decreased by a small amount $\pm\Delta T \approx \pm 0.1T$ at age t_w. The trajectories are then time-averaged over the time $t_{obs} \ll t_w$ spent at $T \pm \Delta T$.

This procedure yields

$$C_V^{\,b}(T) = \frac{\overline{E(T + \Delta T;t_w)} - \overline{E(T - \Delta T;t_w)}}{2\Delta T} \qquad (4)$$

Finally, we gauge the variance of the energy fluctuations within the observation interval $I = [t_w, t_w + t_{obs}]$ and estimate the heat capacity as

$$C_V^{\,c}(T) = \frac{\langle \overline{E^2} - \overline{E}^2 \rangle}{k_B T^2} \qquad (5)$$

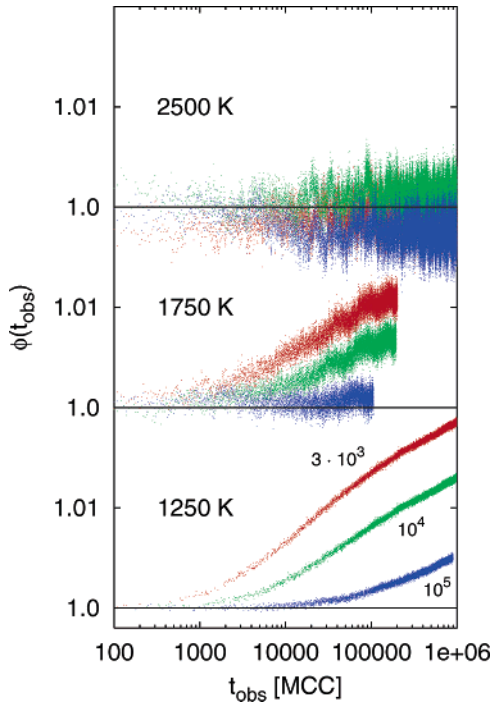

Figure 3. Energy self-correlation functions $\phi(t_{obs})$ for three different temperatures 1250, 1750, and 2500 K (bottom to top). Red, green, and blue curves were recorded after waiting times $t_w = 3 \times 10^3$, 10^4, and 10^5 MCC, respectively. The ensemble averages were calculated over 5 (1750 K), 6 (2500 K), and 100 (1250 K) different trajectories. The number inside the lower figure indicates waiting times t_w (in MCC) after which measurements of $\phi(t_{obs})$ began.

for a range of observation times t_{obs} that straddles t_w. Figure 2, where all C_V values are on a per atom basis, shows that all three expressions agree for temperatures above 3000 K but clearly disagree below 2000 K, which leads to a provisional value for the ergodicity breaking temperature $T_c \approx 2500$ K.

Within the nonergodic region $T < T_c$, we have studied $C_V^a(T)$ for $t_{obs} \ll t_w$, the quasi-equilibrium regime, and for $t_{obs} \gg t_w$, the nonequilibrium regime. The dependence of $C_V^a(T)$ on T, t_{obs}, and t_w can also be obtained from the fitted time and age dependence of the mean energy given in eq 7 below, by performing the time average and then differentiating with respect to T. For $T < T_c$ and $t_{obs} \gg t_w$, we find that C_V^a has a small dependence on the length of the time interval t_{obs} over which the time average is performed. This is connected to the logarithmic drift of the energy, which moreover is more pronounced just below T_c than near $T = 0$ (cf. Figure 4).

C_V^b mimics an experiment performed after some relatively long equilibration time $t_w \gg t_{obs}$ and thus yields the most "realistic" value for the specific heat for all temperatures. C_V^c provides a way to check the validity of the fluctuation−dissipation theorem; it should coincide with the two other expressions above T_c and, additionally, below T_c in the restricted quasi-equilibrium region $t_{obs} < t_w$. Indeed, when t_{obs} is increased past t_w, the observed dynamics in C_V^c change from quasi-equilibrium to off-equilibrium in the temperature range between 2000 and 3000 K (cf. inset in Figure 2). Recall that the (trivial) contribution to C_V due to the change in kinetic energy is never included, i.e., in equilibrium $C_V \to 1.5k_B$ for $T \to 0$ K. Furthermore, the interaction potential $V(r)$ vanishes for $r \to \infty$, and thus this contribution to C_V goes to 0 as $T \to \infty$.

As shown in Figure 2, the above prescriptions for the specific heat yield, as expected, almost identical results in the high-temperature ergodic dynamic regime but differ at low temperature. This indicates that ergodicity is broken below $T_c \approx 2000-3000$ K. Even in the low-temperature region, C_V^b and C_V^c nevertheless roughly coincide over a restricted time interval that corresponds to the quasi-equilibrium regime $t_{obs} < t_w$. However, the inset clearly shows the large difference between C_V^c in the quasi-equilibrium and the nonequilibrium regime, for temperatures below T_C.

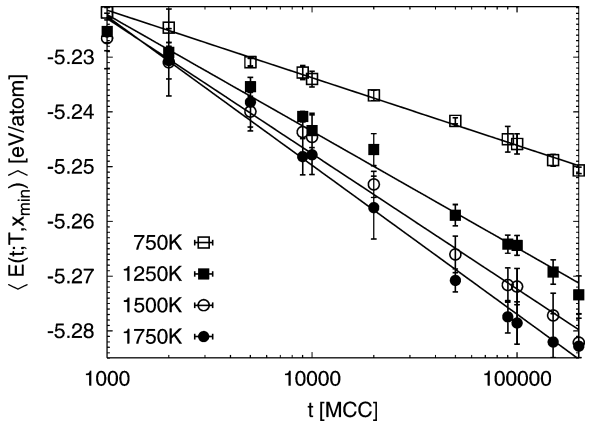

Figure 4. Time dependence of the average energies $\langle E(t;T,x_{min}) \rangle = \langle E_{IS}(t,t_w = t_{init};T) \rangle$ of the minima x_{min} for selected temperatures $T =$ 750, 1250, 1500, and 1750 K as function of time $t = t_{init} + t_{obs}$.

Yet another probe of ergodicity breaking is the two-time energy average defined by

$$\phi(t_w,t_{obs};T) = \frac{\langle E(t_w)E(t_w+t_{obs}) \rangle}{\langle E(t_w)E(t_w) \rangle} \qquad (6)$$

Above T_c and for $t_{obs} < t_w$ below T_c, we expect the dynamics to be time translational invariant, and hence $\phi = 1$. Considering that the energy is negative and decreases monotonically with age, we expect an increase of ϕ with observation time, once the dynamics gain access to states of considerably lower energies.

Figure 3 depicts ϕ for three temperatures, $T = 1250$ K, $T = 1750$ K, and $T = 2500$ K, and for three values of the system age, $t_w = 3 \times 10^3$, 10^4, and 10^5 MCC. The comparison clearly shows that ergodicity is broken as described at the lowest temperature ($T = 1250$ K); due to the decrease in the configurational energy during aging, the two-time energy average increases as the observation time increases. At the intermediate temperature ($T = 1750$ K), the aging effect is still visible but difficult to quantify, and at the highest temperature ($T = 2500$ K), it has vanished completely.

Taking all theses indicators, MSD, BSP, $C_V^{a,\,b,\,c}$, and ϕ into account, we conclude that a-$Si_3B_3N_7$ exhibits ergodicity breaking at $T_c \approx 2000$ K.

3.2. Aging Properties. To describe the nonergodic regime in more detail we have studied the age dependence of (i) the energy of the inherent structures and of the mean potential energy, (ii) the BSP, (iii) the MSD of the particles, and (iv) the two-point correlation function ϕ and the closely related energy−energy autocorrelation function.

The ensemble-averaged energy $\langle E_{IS}(t_w,t) \rangle$ of the inherent structures lying "below" the trajectories observed in the interval $[t_w,t_w + t_{obs}]$ decreases logarithmically with t_{obs}, as does the mean potential energy $\langle E(t_w, t_{obs}) \rangle$. In both cases, the logarithmic slope has a clear temperature dependence but no significant t_w dependence for $t_w \geq t_{init} = 10^3$ MCC. The energy simply decreases logarithmically with the simulation time elapsed after

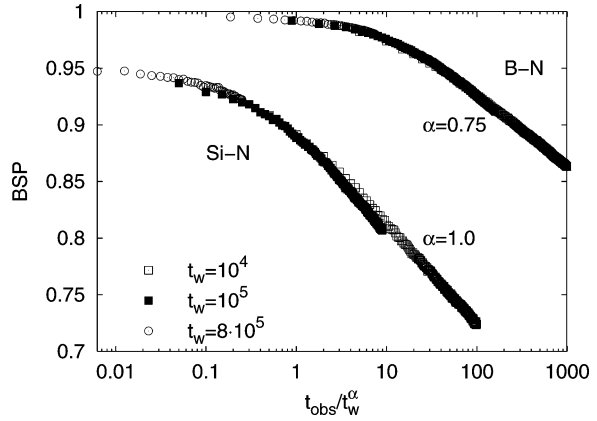

Figure 5. Aging dependence of the bond survival probability BSP for Si−N and B−N bonds, respectively, as a function of t_{obs}/t_w^{α}, at temperature $T = 1250$ K.

the quench, i.e., to a good approximation we find the functional form

$$E(t_{obs};T) = E_0(T) - A(T)\ln\left(\frac{t_{obs} + t_{init}}{t_{init}}\right) \qquad (7)$$

Here, $E_0(T) = \langle E(t_{init};T)\rangle$, and $E_0(T) = \langle E_{IS}(t_{init};T)\rangle$ for potential energies E and minimum energies E_{IS}, respectively, and

$$A_{IS}(T) \approx 6.60 \times 10^{-6}\,T \quad A_E \approx 6.64 \times 10^{-6}\,T \qquad (8)$$

where the coefficients are measured in eV/(K atom). Note that energies are reported on a per atom basis.

The logarithmic decay of the energies is shown in Figure 4 and has previously been observed in other aging systems, see, for example, refs 10 and 51−54.

Bond survival probabilities at $T = 1250$ K for Si−N and B−N bonds are plotted in Figure 5 as a function of the scaled variable t/t_w^{α} for three different ages $t_w = 10^4$, 10^5, 8×10^5 MCC. Even though the data collapse is not perfect, the scaling plots demonstrate that the bonds become, on average, more resilient as the age increases. For the Si−N bond, the best collapse is obtained for $\alpha_{SiN} = 1$. Thus, the survival probability for the Si−N bond is a function of t/t_w, a so-called pure aging behavior. The survival probability for the B−N bond, however, shows a subaging behavior with $\alpha_{BN} = 0.75$. For both types of bonds, the survival probability decays in a logarithmic fashion after a nearly flat initial part, and no cutoff is reached at low temperatures, within the time scale of the simulations. (For temperatures different from 1250 K, the scaling exponents α can only be approximately determined due to the small ensemble of simulation runs at these temperatures. The values for α lie in the range between 0.3 and 0.8.)

Another quantity that exhibits an age dependence for $T < T_C$ is the average mean-square displacement of the atoms, given in eq 1. We observe a subdiffusive behavior, $\mathrm{MSD}(t_{obs},t_w) \propto t_{obs}^{\beta}$ with $\beta < 1$ ($\beta = 1$ corresponds to standard diffusion), in the quasi-equilibrium region ($t_{obs} \ll t_w$).

The MSD remains subdiffusive for $t_{obs} > t_w$ but with an increase in the exponent β. In Figure 6, we show the mean-square displacement $\mathrm{MSD}(t_{obs},t_w)$ for three different waiting times t_w, at temperature $T = 1250$ K. For $t_{obs} \ll t_w$, we find $\beta = 0.5$, and the curves can be approximately collapsed (cf. Figure 6) if t_{obs} is scaled with t_w^{α}. The exponent $\alpha = 0.3$ indicates a strong subaging behavior of the mean-square displacement. This analysis was performed separately for all

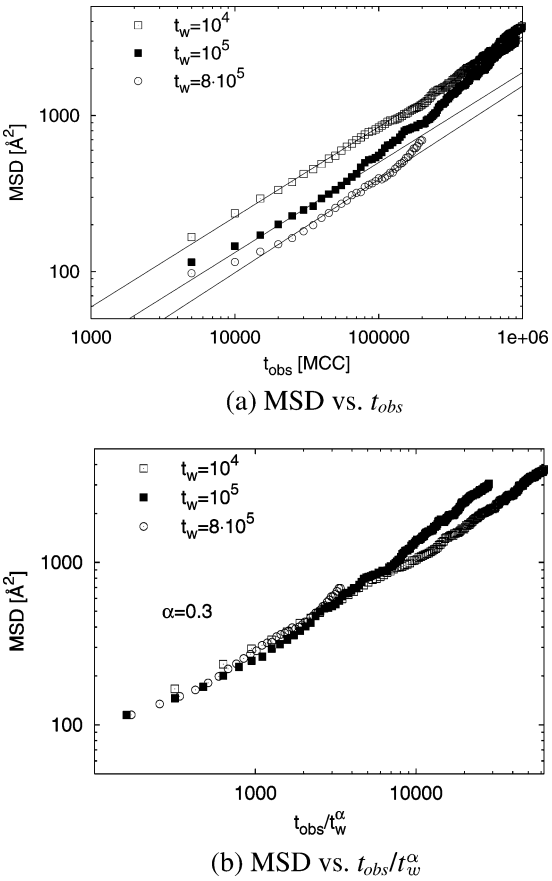

Figure 6. Double logarithmic plot of the mean-square displacement as a function of observation time t_{obs} for different waiting times t_w, at temperature $T = 1250$ K. The exponent $\beta \approx 0.5$ of the subdiffusive motion $\mathrm{MSD} \propto t_{obs}^{\beta}$ for waiting time t_w is found by a fit of the data to a straight line, where only points up to the waiting time t_w were included. β appears to be approximately independent of waiting time for $t_{obs} < t_w$. Although the collapse of the curves after t_w^{α} scaling in part b is not perfect, due to the fact that β starts increasing for $t_{obs} > t_w$, the data indicate strong subaging to be present.

three types of atoms, Si, B, and N. In all three cases, essentially the same results were found.

The two-point correlation function $\phi(t_w,t_{obs};T)$ (cf. Figure 3) remains very close to the equilibrium value 1 in the ergodic temperature region ($T = 2500$ K) and does not depend on waiting time. But in the glassy phase ($T = 1750$ K and $T = 1250$ K), $\phi(t_w,t_{obs};T)$ strongly deviates from its equilibrium value ($\phi \equiv 1$) for $t_{obs} \geq t_w$. Quasi-equilibrium behavior is only observed for observation times $t_{obs} < t_w$ that grow monotonically with t_w. (The closely related autocorrelation function $C_E(t_w,t_{obs};T) \equiv \langle E(t_w)E(t_w + t_{obs})\rangle - \langle E(t_w)\rangle\langle E(t_w + t_{obs})\rangle$ also exhibits the expected aging behavior, i.e., C_E decreases to 0 from an almost constant value ($\propto C_V(t_w)$) once t_{obs} exceeds t_w. Unfortunately, the data is too noisy for us to draw any quantitative conclusions, beyond the observation that the quasi-equilibrium regime grows monotonically with t_w.)

This monotonic dependence on t_w of the time range during which the quasi-equilibrium behavior is still observed correlates with the stiffening of the response of the system characteristic for aging processes. The longer the system is allowed to equilibrate, the longer the subsequent time range during which equilibrium-like behavior is observed. This effect concurs with the logarithmic decay of $E(t;T)$ and $\langle E(t;T)\rangle$ (cf. Figure 4) and fully agrees with the general aging behavior previously discussed.

Discussion

Numerical investigations of atomistic models with realistic interactions are computationally very demanding, and for the same numerical effort, the accuracy of the results obtained is lower than what can be achieved for more simplified models. Despite this limitation, we have shown how ergodicity is broken in a-$Si_3B_3N_7$ and have characterized the dynamics in the low-temperature phase, where the model behaves as a bona fide aging system. In the aging regime, the microscopic time scale of the dynamics is largely irrelevant and so is the precise value of the conversion factor between the time scales of Monte Carlo and molecular dynamics simulations. This assumption is supported by the fact that we have observed a similar slow drift in energy at low-temperature MD simulations, i.e., in the nonergodic regime, during studies of heat transport in a-$Si_3B_3N_7$.[55] Therefore, we trust that the qualitative and most of the quantitative aspects of our findings can be carried over to the real materials.

The computational analysis of a-$Si_3B_3N_7$ using MSD, BSP, C_V[a,b,c], and $\phi(t_w,t_{obs};T)$ shows that this amorphous material can be expected to exhibit a glass transition with a concurrent break in the ergodicity at about $T_c \approx 2000$ K if pressures high enough to prevent decomposition are applied. (Repeating these investigations for a large number of densities, we always find a similar freezing-in of the structure for $T \approx T_c$. In other work, we have determined a critical point in the liquid−gas region of the ternary system ($p_{cr} \approx 1.3$ GPa and, $T_{cr} \approx 8000$K).[39] Since the tendency to decompose is greatly reduced for a supercritical fluid, we predict that a-$Si_3B_3N_7$ should exhibit a glass transition at a temperature $T_G \approx 1700-2500$ K and at a pressure of $p_G > 2$ GPa. Up to now, high-pressure experiments have only been performed for $T \approx 1000$ K and $p \approx 2.5$ GPa.)

For $T < T_c$, a-$Si_3B_3N_7$ exhibits a general behavior in many respects similar to standard test systems for computer simulations[12,43,44] (Lennard-Jones, a-SiO_2), insofar as we observe a freezing-in of the structure, a logarithmic decay of the energy, and a systematic waiting time dependence of the bond survival probability, the mean-square displacement of the particles, and the two-time energy correlation function.

The aging behavior of the heat capacity has been studied experimentally, for charge-density wave systems[46] and for a spin-glass model,[22] and discussed theoretically for two-level systems at very low temperatures.[56]

The logarithmic drift toward lower energies occurring for $T < T_c$ is also observed in a number of model systems such as Lennard-Jones[51] and soft-sphere glasses.[52] This applies to both the actual trajectories and the time sequence of observed local minima. For a fixed simulation time, the deepest local minima are reached for $T = 1750$ K, which lies right below T_c. Analogous observations are well-known from, e.g., global optimization studies of complex systems, where it has been found that reaching the deepest local minima using Monte-Carlo-type search algorithms is achieved by spending most of the search time in the temperature interval slightly below the glass transition temperature.[57,58] Thus, this result provides another confirmation that ergodicity breaking takes place at $T \approx T_c$.

In summary, all of the numerical evidence obtained from our simulations shows that the thermal quench of a-$Si_3B_3N_7$ melt produces a material in a state of strong thermodynamic disequilibrium, which then relaxes through the aging process. As we have noted in the Introduction, a-$Si_3B_3N_7$ is currently only synthesized via the sol−gel route. In earlier work,[59] we have shown that different synthesis routes (quench from melt, sol−gel, sintering of nanocrystallites, etc.) result in amorphous compounds that exhibit a monotonic decrease in energy during simulations at $T < 2000$ K. This applies in particular to the relaxation of the structures that results from modeling the sol−gel synthesis route,[60,61] as we observed in both constant volume and constant pressure simulations.[62] Thus, we surmise that aging phenomena analogous to those investigated here for a quenched melt also occur in the amorphous ceramic generated via the sol−gel route.

The metastable states reached during aging become gradually lower in energy, which could lead to a strengthening of the material. However, the structural transformations that would accompany aging could lead to the formation of nanocrystallites and internal "grain boundaries", whence the overall structure might develop, e.g., cracks and thus lead to a weakening of the mechanical properties of the material. This could especially be the case if crystallites of binary or ternary phases are formed. However, for most envisaged applications, the time scales on which such processes might occur are beyond the accessible simulation time by many orders of magnitude.

Acknowledgment. Funding was kindly provided by the DFG via Grant No. Sonderforschungsbereich 408.

References and Notes

(1) Turnhout, J. V.; Klaase, P. T. A.; Ong, P.; Struik, L. *J. Electrostat.* **1977**, *3*, 171−179.
(2) Struik, L. *Physical Aging in Amorphous Polymers and Other Materials*; Elsevier Science Ltd: New York, 1978.
(3) Lundgren, L.; Svedlindh, P.; Nordblad, P.; Beckman, O. *Phys. Rev. Lett.* **1983**, *51*, 911−914.
(4) *Spin Glasses and Random Fields*; Young, A. P., Ed.; World Scientific: Singapore, 1998.
(5) Alba, M.; Ocio, M.; Hammann, J. *Europhys. Lett.* **1986**, *2*, 45−52.
(6) Nordblad, P.; Svedlindh, P.; Lundgren, L.; Sandlund, L. *Phys. Rev. B* **1986**, *33*, 645−648.
(7) Alba, M.; Hammann, J.; Ocio, M.; Refregier, P. *J. Appl. Phys.* **1987**, *61*, 3683−3688.
(8) Svedlindh, P.; Granberg, P.; Nordblad, P.; Lundgren, L.; Chen, H. *Phys. Rev. B* **1987**, *35*, 268−273.
(9) Nicodemi, M.; Jensen, H. J. *J. Phys. A: Math. Gen.* **2001**, *34*, 8425.
(10) Kob, W.; Barrat, J.; Sciortino, F.; Tartaglia, P. *J. Phys.: Condens. Matter* **2000**, *12*, 6385−6394.
(11) Utz, M.; Debenedetti, P. G.; Stillinger, F. H. *Phys. Rev. Lett.* **2000**, *84*, 1471−1474.
(12) Barrat, J. L.; Kob, W. *J. Phys.: Condens. Matter* **1999**, *11*, A247−A252.
(13) Barrat, J. L. ; Berthier, L. *Phys. Rev. E* **2001**, *63*, 012503.
(14) Berthier, L.; Bouchaud, J.-P. *Phys. Rev. B* **2002**, *66*, 054404.
(15) Josserand, C.; Tkachenko, A. V.; Mueth, D. M.; Jaeger, H. M. *Phys. Rev. Lett.* **2000**, *85*, 3632−3635.
(16) Cipelletti, L.; Manley, S.; Ball, R. C.; Weitz, D. A. *Phys. Rev. Lett.* **2000**, *84*, 2275−2278.
(17) Bissig, H.; Romer, S.; Cipelletti, L.; Trappe, V.; Schurtenberger, P. *Phys. Chem. Commun.* **2003**, *6*, 21−23.
(18) Cipelletti, L.; Bissig, H.; Trappe, V.; Ballesta, P.; Mazoyer, S. *J. Phys.: Condens. Matter* **2003**, *15*, S257−S262.
(19) Buisson, L.; Bellon, L.; Ciliberto, S. *J. Phys.: Condens. Matter* **2003**, *15*, S1163.
(20) Buisson, L.; Ciliberto, S.; Garciamartin, A. *Europhys. Lett.* **2003**, *63*, 603.
(21) Sibani, P.; Dall, J. *Europhys. Lett.* **2003**, *64*, 8−14. Sibani, P.; Dall, J. *Europhys. Lett.* **2005**, *69*, 563−569.
(22) Sibani, P.; Jensen, H. J. *Europhys. Lett.* **2004**, *69*, 563−569; see cond-mat/0403212.
(23) Crisanti, A.; Ritort, F. *Europhys. Lett.* **2004**, *66*, 253−259.
(24) Cugliandolo, L. F.; Kurchan, J.; Peliti, L. *Phys. Rev. E* **1997**, *55*, 3898−3914.
(25) Calabrese, P.; Gambassi, A. cond-mat/0410357.
(26) Bouchaud, J. *J. Phys. I* **1992**, *2*, 1705−1713.
(27) Rinn, B.; Maass, P.; Bouchaud, J. P. *Phys. Rev. B* **2001**, *64*, 104414.
(28) Jansen, M.; Jäschke, B.; Jäschke, T. In *Structure & Bonding*; Jansen, M., Ed.; Springer-Verlag: Berlin, 2002; Vol. 101, Chapter 1, pp 138−191.
(29) Seyferth, D.; Plenio, H. *J. Am. Ceram. Soc.* **1990**, *73*, 2131.

(30) Baldus, H. P.; Wagner, O.; Jansen, M. In *Materials Research. Society Symposium Proceedings*; Hampden-Smith, M. J., Klemperer, W. G., Brinker, C. J., Eds.; Materials Research Society: Warrendale, PA, 1992; Vol. 271.

(31) Su, K.; Remsen, E.; Zank, G.; Sneddon, L. *Chem. Mater.* **1993**, *5*, 547.

(32) Funayama, O.; Kato, T.; Tashiro, Y.; Isoda, T. *J. Am. Ceram. Soc.* **1993**, *76*, 717.

(33) Jansen, M.; Baldus, P. *Angew. Chem., Int. Ed. Engl.* **1997**, *36*, 328−344.

(34) Baldus, P.; Jansen, M.; Sporn, D. *Science* **1999**, *285*, 699−703.

(35) Aldinger, F.; Weinmann, M.; Bill, J. *Pure Appl. Chem.* **1998**, *70*, 439.

(36) Srivastava, D.; Duesler, E.; Paine, R. *Eur. J. Inorg. Chem.* **1998**, *6*, 855.

(37) Riedel, R.; Kienzle, A.; Dressler, W.; Ruwisch, L.; Bill, J.; Aldinger, F. *Nature* **1996**, *382*, 796.

(38) van Wüllen, L.; Müller, U.; Jansen, M. *Angew. Chem., Int. Ed.* **2000**, *39*, 2519−2521.

(39) Hannemann, A.; Schön, J.; Jansen, M. *Phys. Rev. E*, submitted for publication.

(40) Casas-Vazquez, J.; Jou, D. *Rep. Prog. Phys.* **2003**, *66*, 1937−2023.

(41) Horbach, J.; Kob, W. *Phys. Rev. B* **1999**, *60*, 3169−3181.

(42) Stillinger, F.; Weber, T. A. *Phys. Rev. A* **1982**, *25*, 978−989.

(43) Sastry, S.; Debenedetti, P. G.; Stillinger, F. H.; Schroder, T. B.; Dyre, J. C.; Glotzer, S. C. *Physica A* **1999**, *270*, 301−308.

(44) Crisanti, A.; Ritort, F. *Europhys. Lett.* **2000**, *52*, 640−646.

(45) Nordblad, P.; Svendlidh, P. In *Spin Glasses and Random Fields*; Young, A., Ed.; World Scientific: Singapore, 1997; Chapter 1, pp 1−28.

(46) Biljakovic, K.; Lasjaunias, J.; Monceau, P.; Levy, F. *Phys. Rev. Lett.* **1991**, *67*, 1902−1905.

(47) Gastreich, M.; Marian, C.; Gale, J. *Phys. Rev. B* **2000**, *62*, 3117−3123.

(48) Huitema, H.; van der Eerden, J. P. *J. Chem. Phys.* **1999**, *110*, 3267−3274.

(49) Elliott, S. R. *Physics of Amorphous Materials*; Longman Scientific & Technical: Essex, U. K., 1990.

(50) Yu, C. C.; Carruzzo, H. M. *Phys. Rev. E* **2004**, *69*, 051201.

(51) Kob, W.; Sciortino, F.; Tartaglia, P. *Europhys. Lett.* **2000**, *49*, 590−596.

(52) Angelani, L.; Di Leonardo, R.; Parisi, G.; Ruocco, G. *Phys. Rev. Lett.* **2001**, *87*, 5502−5506.

(53) Kob, W.; Barrat, J. L. *Eur. Phys. J. B* **2000**, *13*, 319−333.

(54) Dall, J.; Sibani, P. *Eur. Phys. J. B* **2003**, *36*, 233−243.

(55) Schön, J. C.; Hannemann, A.; Sethi, G.; Jansen, M.; Salamon, P.; Frost, R.; Kjeldgaard, L. In *Proceedings of the Workshop on "Structure and Kinetics of Nucleation and Crystallization in Noncrystalline Materials"*, Jena, Germany, Sept 2002; see also cond-mat/0212279.

(56) Parshin, D.; Sahling, S. *Phys. Rev. B* **1993**, *47*, 5677−5688.

(57) Kirkpatrick, S.; Gelatt, C. D., Jr.; Vecchi, M. P. *Science* **1983**, *220*, 671−680.

(58) Salamon, P.; Sibani, P.; Frost, R. *Facts, Conjectures, and Improvements for Simulated Annealing*; SIAM Monographs: Philadelphia, PA, 2002.

(59) Hannemann, A.; Schön, J. C.; Putz, H.; Lengauer, T.; Jansen, M. *Phys. Rev. B* **2004**, *70*, 144201.

(60) Schön, J. C.; Hannemann, A.; Jansen, M. *J. Phys. Chem. B* **2004**, *108*, 2210−2217.

(61) Hannemann, A.; Schön, J. C.; Jansen, M. *J. Mater. Chem.* **2005**, *15*, 1167−1178.

(62) Hannemann, A.; Schön, J. C.; Jansen, M. *Philos. Mag.*, in press.